PAPER • OPEN ACCESS

Recent progress towards a physics-based understanding of the H-mode transition

To cite this article: G R Tynan *et al* 2016 *Plasma Phys. Control. Fusion* **58** 044003

View the article online for updates and enhancements.

Recent progress towards a physics-based understanding of the H-mode transition

G R Tynan[1]**, I Cziegler**[1]**, P H Diamond**[1,2]**, M Malkov**[2]**, A Hubbard**[3]**,
J W Hughes**[3]**, J L Terry**[3] **and J H Irby**[3]

[1] Center for Momentum Transport & Flow Organization (CMTFO), University of California San Diego, La Jolla, CA 92093, USA
[2] Center for Astrophysics & Space Science, University of California San Diego, La Jolla, CA 92093, USA
[3] MIT Plasma Science and Fusion Center, Cambridge, MA 02139, USA

E-mail: gtynan@ucsd.edu

CrossMark

Abstract

Results from recent experiment and numerical simulation point towards a picture of the L-H transition in which edge shear flows interacting with edge turbulence create the conditions needed to produce a non-zero turbulent Reynolds stress at and just inside the LCFS during L-mode discharges. This stress acts to reinforce the shear flow at this location and the flow drive gets stronger as heating is increased. The L-H transition ensues when the rate of work done by this stress is strong enough to drive the shear flow to large values, which then grows at the expense of the turbulence intensity. The drop in turbulence intensity momentarily reduces the heat flux across the magnetic flux surface, which then allows the edge plasma pressure gradient to build. A sufficiently strong ion pressure gradient then locks in the H-mode state. These results are in general agreement with previously published reduced 0D and 1D predator prey models. An extended predator–prey model including separate ion and electron heat channels yields a non-monotonic power threshold dependence on plasma density provided that the fraction of heat deposited on the ions increases with plasma density. Possible mechanisms to explain other macroscopic transition threshold criteria are identified. A number of open questions and unexplained observations are identified, and must be addressed and resolved in order to build a physics-based model that can yield predictions of the macroscopic conditions needed for accessing H-mode.

Keywords: turbulence, h-mode, L-H transition, predator–prey, Reynolds stress

(Some figures may appear in colour only in the online journal)

Introduction

Since its discovery in 1982 [1], the high confinement (H-mode) regime has been found to occur in all large-scale fusion devices, and forms the baseline operational scenario for ITER. The key role that $E \times B$ sheared flows associated with the ion pressure gradient play in sustaining the H-mode has been well documented [2], but the mechanism that initiates the onset of the H-mode has remained elusive. As discussed in

a recent review article [3], the key initiating event appears to be a transient in the poloidal plasma velocity in the regime just inside (~1 cm) the last closed flux surface (LCFS). Given the significance of this regime for planned ITER operations, as well as the underlying interesting fundamental physics, there is a strong motivation to obtain a deeper understanding of the origin of the H-mode transition.

The conditions for accessing the H-mode have been explored across many devices and the results have been used to formulate empirical scaling laws to access the H-mode regime. These studies usually define a minimum heating power threshold, P_{th}, which must be reached in order for the L-mode to H-mode (L-H) transition to occur. The power

threshold is then expressed in terms of macroscopic quantities like plasma density, magnetic field, plasma current, edge safety factor, and so on (see, e.g. Martin [4] for one such analysis). In addition, experiments show that the threshold is lower when the ion grad-$B \times B$ direction points towards the X-point in a single null divertor [5], and that P_{th} is influenced by the X-point height from the divertor target and wall cleanliness [6]. These empirical approaches have formed the primary means by which access conditions for, e.g. ITER are predicted. However, these approaches have significant uncertainties associated with them, and thus the conditions necessary to operate in H-mode are also correspondingly uncertain. A more physics-based approach to predicting the H-mode access conditions might then also reduce this uncertainty.

Background

Earlier experimental work in the ASDEX-UPGRADE device (AUG) [7] clearly showed the existence of an oscillatory regime when operating at heat fluxes that were close to the power threshold. At about the same time, theory [8] proposed that the turbulence-driven Reynolds stress could act to amplify a pre-existing shear flow by nonlinearly driving the shear flow to large amplitude. Because of its similarity to such sheared flows in the core of the plasma, as well as to geophysical fluid systems, here we shall refer to this flow as a turbulent driven zonal flow (ZF). In this theory, the increase in ZF energy came at the expense of the turbulence energy, and thus the turbulence amplitude would die away as the ZF amplitude grew. However, once the turbulent drive was weak enough, the ZF would damp away in this model and, in the absence of any other mechanism to keep the turbulence level suppressed, the turbulence intensity would then recover. As a result, the system would execute a limit-cycle type behavior, and would not stay in a state of reduced turbulence/strong shear flow akin to the H-mode regime. Experiments in DIII-D [9] were interpreted in a similar vein, in which a growing fluctuation amplitude would in turn drive a sheared $E \times B$ flow that, in turn, acted to quench the turbulence, and resulted in a limit cycle behavior.

This predator–prey model was then modified to include the effect of a sheared flow associated with the ion pressure profile [10]. The essential new element of this model was the inclusion of a so-called mean shear flow (MSF) that can be sustained even in the absence of turbulent flow drive. As a result, when operating at conditions close to the threshold for transition, this new model could exhibit limit cycle oscillations (LCOs), between regimes of high turbulence/weak ZF and low amplitude turbulence/strong ZF. However, further increases in heat flux through the system would increase the MSF to the point where it was strong enough to maintain a state of reduced turbulence. In this case, since the cross-field heat flux was taken to be proportional to the turbulence intensity, a steep edge pressure gradient would form at the apex of the LCO regime, and lock-in a state of high confinement that could be maintained indefinitely.

Work on TJ-II showed that the mean E_r did not evolve prior to the L-H transition in that device, but the reported observation mentioned that low-frequency (1–10 kHz) E_r fluctuations could in fact evolve shortly before the transition [11]. Subsequent work on TJ-II by Estrada and coworkers [12] demonstrated that a LCO regime between the L-mode and H-mode states that was characterized by an oscillation in the sheared $E \times B$ flow and the turbulence amplitude existed in the region located just inside the LCFS. The data were interpreted to be consistent with the predator prey picture. More recent work on TJ-II [13] extended these studies to include one-dimensional (1D) effects, which showed evidence for radial propagation of the turbulence intensity and shear flow evolution. As a result of these 1D effects, the detailed turbulence intensity-shear flow phase space orbit dynamics can exhibit complex behaviors, including reversals in the direction of the phase space orbit at different positions.

Work in the AUG [14] and DIII-D [15] tokamak devices provided significant additional insights into the oscillatory regime lying between the L-mode and H-mode states. Both works show the formation of an oscillatory $E \times B$ shear flow in the region just inside the LCFS together with modulation of the turbulence intensity in the same region of the plasma. In DIII-D, the modulations occur initially with a frequency of ~2 kHz. Over the number of these oscillations, the background plasma pressure gradient was observed to slowly grow, and the oscillation period became gradually longer. Eventually one large final burst of shear flow would occur, the turbulence would collapse, and the H-mode state then ensued. In the AUG, the dynamics were different. Again, LCO-type oscillations would occur. However, in the time windows in which turbulence suppression would occur, the sheared $E \times B$ flow was modulated at a significantly higher frequency, possibly associated with the geodesic acoustic mode (GAM). These windows of strong $E \times B$ activity would occur with a frequency of about 1 kHz, and the sheared $E \times B$ drift would oscillate. Over a significant number of these windows, the background $E \times B$ shear flow strength was found to increase. Eventually it then became strong enough to lock in the H-mode state, in a manner reminiscent of the results reported by Schmitz. More recently, work in EAST [16] has also shown similar essential features during the L-mode/LCO/H-mode transition in that device.

These studies provide strong experimental evidence in support of the predator–prey model [10, 17–19]. However, these earlier experimental studies did not directly address the underlying physics of the model, namely the nonlinear transfer of kinetic energy from the turbulent scale to the ZF scale, and the subsequent collapse of the turbulence, which then sets up the conditions necessary for the formation of a steep pressure gradient.

This paper aims to provide an up-to-date picture of the status of our understanding of the origin of the L-H transition, and in particular provide a detailed test of the hypothesis that turbulent driven shear flows act to trigger the H-mode. The approach taken in the experimental work discussed below attempts to make direct measurements of the key turbulence physics quantities underlying the theory. In order to do so, this paper presents a combination of recent work in HL-2A together with a number of new results from the ALCATOR

C-Mod device. Recent theory and modeling then complete the presentation.

This paper is organized as follows. We first use the reduced predator–prey model to motivate a description of the H-mode transition written in terms of the more primitive turbulent stress and the associated Reynolds work done by the turbulence on the shear flow. This model provides expressions that can directly be evaluated with suitable turbulence data. Second, we examine the evolution of turbulent-shear flow coupling in steady-state L-mode discharges that have increasing levels of heating that approach the L-H transition threshold. Those results, obtained in both limiter discharges on HL-2A and single null ALCATOR C-Mod diverted discharges show that the turbulence acts to reinforce the sheared $E \times B$ flow that exists just inside the last closed flux surface (LCFS), and that the turbulent drive of the shear flow gets stronger as the heating is increased. Third, we then examine the fast (~1 ms) transient evolution of the turbulence, turbulent Reynolds stress, and turbulent flow drive during fast L-H transition in ALCATOR C-Mod. The results show that a rapid increase in the turbulent stress and turbulent flow drive occurs just before the L-H transition, and that this transient is localized to the region immediately inside the LCFS. Furthermore, the measurements show that the flow drive momentarily becomes strong enough to extract most of the fluctuation kinetic energy. This then leads to the turbulence amplitude collapse. The edge pressure gradient then builds in response, and locks in the H-mode state. Fourth, we compare these experimental results against recently published turbulent fluid models of the formation of an edge transport barrier, and point out the similarities between the experiment and simulations. Fifth, we then summarize recent theory work that extends the predator–prey model by separating out the electron and ion heat transport channels separately. This model can then provide a qualitative explanation for the non-monotonic dependence of the macroscopic H-mode power threshold on line-averaged density. Finally, we summarize observations in other devices that suggest there is no role for turbulent-induced sheared flows at the L-H transition, and that instead the sheared $E \times B$ flow is either consistent with the ion pressure gradient alone (i.e. the so-called ion diamagnetic $E \times B$ flow), or is consistent with ion orbit loss mechanisms. We also point out theory arguments that toroidal flow damping caused by geodesic acoustic modes should provide strong damping of these effects. The paper then closes with suggestions for future work to try to resolve these apparent discrepancies.

Model summary

In order to design experiments and diagnostic/data analysis schemes that could be used to attempt to directly measure the turbulent stress and address its possible role in initiating the H-mode transition, the predator–prey model was then recast into a more primitive turbulent K-ε framework [20–23] that expressed the evolution of the turbulent and ZF scale kinetic energy explicitly in terms of the underlying turbulent flow production rate that is mediated by the Reynolds work done

by the turbulence on the sheared ZF. In a simplified form, these two energy scales evolve according to the model

$$\frac{\partial \widetilde{K}}{\partial t} = (\gamma_{\text{in}} - \gamma_{\text{corr}}^{\text{pl}})\widetilde{K} - P - \partial_r \widetilde{T}$$

$$\frac{\partial \overline{K}}{\partial t} = P - \partial_r \overline{T} - \nu_{\text{LF}}\overline{K}$$

where the terms are given as

$$\widetilde{K} = \frac{1}{2}\langle \tilde{v}^2 \rangle \quad \overline{K} = \frac{1}{2}\langle V^{\text{LF}} \rangle^2$$

$$P = \langle \tilde{v}_r \tilde{v}_\theta \rangle \frac{\partial \langle V^{\text{LF}} \rangle}{\partial r}$$

$$\widetilde{T} = \langle \tilde{v}_r \tilde{v}^2{}_\theta \rangle \quad T = \langle \tilde{v}_r \tilde{v}_\theta \rangle \langle V^{\text{LF}} \rangle$$

$$\gamma_{\text{in}} = \gamma_{\text{in}}(\nabla n, \nabla T, V^{\text{LF}'})$$

$$\langle V^{\text{LF}} \rangle = \langle V_{E \times B} \rangle + \langle V_i^{\text{dia}} \rangle$$

Here $\widetilde{K}, \overline{K}$ denote the kinetic energy on the fluctuation and shear flow scales respectively, P denotes the nonlinear turbulent production of shear flow, $\widetilde{T}, \overline{T}$ denote the radial flux of turbulent intensity and zonal flow intensity, γ_{in} and $\gamma_{\text{corr}}^{\text{pl}}$ denote the growth rate of the underlying instability driving the turbulence and the effective rate of turbulent decorrelation due to high-frequency dissipation effects, respectively, the low-frequency $E \times B$ shear flow and its dissipation rate are given by $V_{E \times B}$ and ν_{LF}, respectively, and the ion diamagnetic drift velocity is given as V_i^{dia} and is related to the ion pressure gradient by the usual definition. Note then that the heat flux through the edge region relates the diamagnetic flow to the mean pressure gradient. Note also that this model implicitly assumes a separation of scales between turbulent timescales and slower so-called 'mean' quantities such as the pressure gradient and ion diamagnetic flow.

A criterion for the collapse of the turbulence energy $\widetilde{K}$ due to its nonlinear transfer of kinetic energy into the sheared $E \times B$ flow is given trivially as

$$R_{\text{T}} \equiv \frac{P + \partial_r \widetilde{T}}{(\gamma_{\text{in}} - \gamma_{\text{corr}}^{\text{pl}})\widetilde{K}} > 1$$

It is expected that once the turbulence collapses, the nonlinear production, P, of the sheared flow will also collapse and the turbulent transport of heat will be reduced significantly. In this case, if the ion diamagnetic flow is able to grow to sufficient magnitude before the turbulent driven shear flow decays away at a rate ν_{LF}, then it can take over the task of turbulence suppression, and a state of reduced turbulence and steepened gradients can be maintained. This is the essential picture contained in the 0D and 1D predator-prey models put into a framework that can be addressed with suitable turbulence data analysis. In the next section, we summarize recent experiments that address the key elements of this picture in both steady-state L-mode discharges that gradually approach the conditions of the L-H transition, as well as experiments in Alcator C-Mod that examine the evolution of the turbulence, the nonlinear shear flow production, and mean gradients
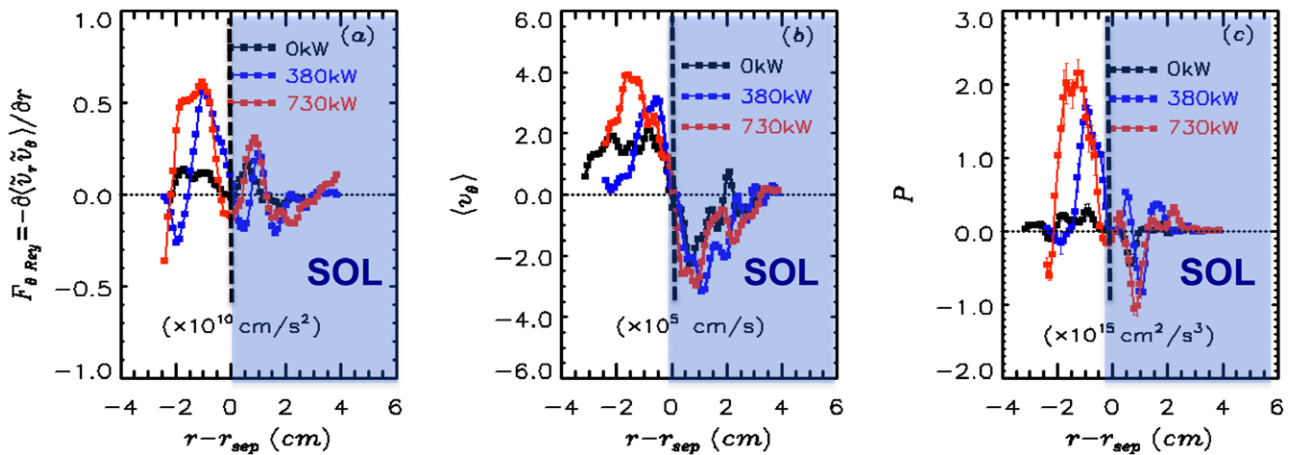
Figure 1. (a) Reynolds force arising from the gradient of the turbulent Reynolds stress, (b) time-averaged radial profile of poloidal flow, (c) nonlinear turbulent flow production, *P*. data from HL-2A ECH heated discharges. Results from the HL-2A device. Figure taken from [22].

during fast L-H transitions. The results provide useful tests of the role of turbulence in initiating the L-H transition.

Turbulence-sheared *E* × *B* flow interactions in L-mode

The existence of a sheared *E* × *B* flow at the LCFS region of toroidally confined plasmas has been known for nearly 30 years and was first demonstrated by studies on the TEXT device [24], and then subsequently in other tokamaks and on other types of confinement devices [25]. Such sheared *E* × *B* flows can act to distort the turbulent eddies found in the edge plasma; in the absence of flow shear they tend to be roughly isotropic in the poloidal plane but with the application of a flow shear they become tilted and stretched [26, 27]. The resulting isopotential contours of the turbulent structures effectively form streamlines of the nearly two-dimensional (2D) turbulent flow field and, as a result of this tilting and stretching, the radial and poloidal velocity fluctuations become correlated, resulting in the formation of a non-zero turbulent Reynolds stress.

Recent experiments in the HL-2A device and Alcator C-Mod show how this process evolves in L-mode as the heating power is increased. A two-dimensional probe array was used in HL-2A to try to measure the turbulent stress, edge plasma shear flow, and the resulting effect on the nonlinear production of sheared *E* × *B* flow by the turbulence. The results (figure 1 below) showed that the shear layer gradually become stronger as ECH heating power was applied to these discharges. Furthermore, the turbulent stress was found to increase and thus the effective Reynolds force applied to the plasma by the turbulence also increased. As a result, the net shear flow production, *P*, also increased in L-mode. A frequency resolved analysis of this process [28] showed that at low power, the power transfer was predominantly to a finite frequency oscillatory *m*, *n* = 0,0 shear flow previously identified as a GAM. As the heating power was increased, the intensity of the drive of both the ZF and the GAM increased. However, the drive of the GAM eventually reached a peak and

then began to decrease, while the ZF drive was found to monotonically increase with increased heating power. Thus these two elements of the edge shear flow compete, but it would appear that with sufficient heating power the ZF becomes the dominant component of the turbulent driven shear flow.

These earlier results were made with Langmuir probes, and are thus subject to the usual concerns about probe measurements in the edge of a tokamak plasma, e.g. does the probe make a large perturbation to the plasma, and are the measurements corrupted by electron temperature fluctuation effects [29]? Motivated in part by these considerations, a similar study has been carried out on the Alcator C-Mod. However, in this work a toroidally localized 2D He gas puff imaging (GPI) diagnostic was used to image the turbulent dynamics across the edge, LCFS and SOL plasma regions. These experiments were carried out in time-stationary L-mode discharges formed with a lower single null and with the ion grad-*B* × *B* drift direction pointing away from the X-point. This effectively raises the power threshold for the H-mode, allowing a wider range of heating power to be applied in time-stationary L-mode conditions. Detailed descriptions of the diagnostic and the data analysis technique can be found elsewhere [30, 31]. The motion of time-resolved 2D light intensity fluctuations is used to estimate a two-dimensional velocity field, and then, once these quantities are determined, the turbulent stress, flow production, and other quantities of interest can be determined.

The model introduced earlier suggests that the turbulence collapse that occurs at the onset of the L-H transition is associated with a power balance on the turbulence scales. Thus, an examination of the turbulent decorrelation rate, which (presumably) indicates the rate at which turbulence energy is dissipated at high frequency/high wavenumber scales, as well as the *rate* of energy transfer into the low-frequency shear flow, is of interest. Because these particular experiments are time-stationary, frequency-resolved Fourier analysis techniques can be used to determine this latter rate. In particular, using previously published bispectral analysis techniques [32], we can write the power transfer into the shear flow at frequency f in terms of the cross-bispectrum
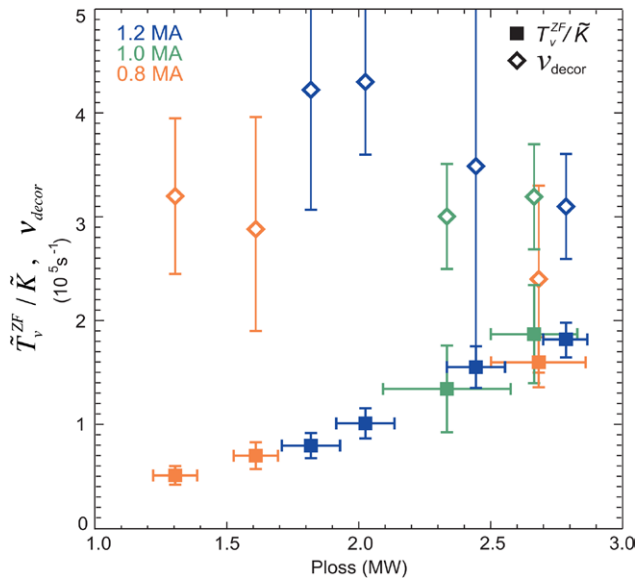
Figure 2. Variation of the plasma-frame turbulent decorrelation rate, ν_{decor}, and the rate of energy transfer into the low-frequency sheared $E \times B$ flow, given by $\nu_{\mathrm{NL}} = T_\nu^{\mathrm{ZF}}/\tilde{K}$. The rate of shear flow drive is found to increase monotonically with increased heat flux at the plasma boundary. Data taken in 5.4 T LSN Alcator C-Mod discharges with ion grad-$B \times B$ drift pointing away from X-point. Heating from ALCATOR C-MOD Ohmic and ICRF heated discharges.

$$T_\nu^{\mathrm{ZF}} = -\mathrm{Re}\left[\sum_{f_1; f=f_{\mathrm{ZF}}} \left\langle \tilde{\nu}_\theta(f)\tilde{\nu}_r(f-f_1)\partial_r\tilde{\nu}_\theta(f_1) \right\rangle \right]$$

where the velocities here are determined from velocimetry analysis of the 2D He-GPI data. The rate of this power transfer, ν_{NL}, is then determined by normalizing the power transfer T_ν^{ZF} by the turbulent kinetic energy, $\nu_{\mathrm{NL}} = \sum_f T_\nu^{\mathrm{ZF}}(f)/\sum_f \frac{1}{2}\tilde{\nu}_\perp^2(f)$. For the purposes of this analysis, the upper bounds of the shear flow frequency is taken as $f = 3\,\mathrm{kHz}$ in this analysis, while the lower bounds of the frequency defining the 'turbulence' frequency band was set to $5\,\mathrm{kHz}$. The results of this analysis from a series of L-mode discharges in C-Mod are shown in figure 2 below. At low heating power, the turbulent decorrelation rate is about an order of magnitude larger than the rate of transfer into the shear flow. As the heating power increases, the rate of energy transfer associated with the nonlinear flow drive increases and, at the highest L-mode powers shown here, begins to approach the turbulent decorrelation rate. At low power, the shear flow has little effect on the turbulent scale power balance and thus, in the model presented above, the turbulence saturation is then determined by a balance of the instability growth rate and the turbulent decorrelation rate. However, as the heating power input is increased, the turbulent decorrelation rate does not change substantially, whereas ν_{NL}, exhibits a pronounced increase and, at the largest L-mode heating powers used in these experiments begins to approach the turbulent decorrelation rate. This result would then indicate that in strongly heated L-mode plasmas, the turbulent shear flow present at the plasma edge begins to play a significant role in the saturation of the turbulence intensity.
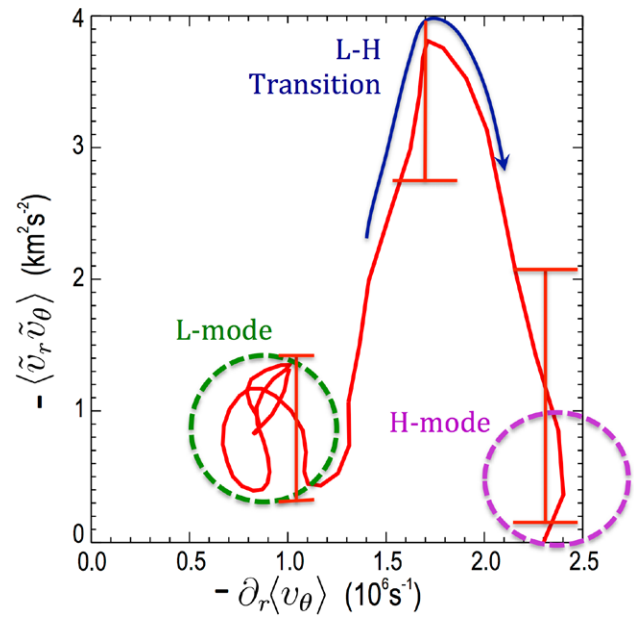
Figure 3. Transient evolution of turbulent stress verses the shearing rate during an L-H transition in ALCATOR C-Mod. The turbulent stress increases markedly as the shear flow begins to grow during the early portion of the L-H transition. As the shearing rate increases further, the turbulent stress reaches a peak value, and then falls as the shearing rate is increased further. The H-mode state then ensues, characterized by a strong shear and a weak turbulent stress.

Turbulent-shear flow interaction during fast L-H transition

These Fourier-domain approaches cannot be used to study the fast transient L-H transition, as the time-stationary assumption is violated. However, working in the time domain, and using knowledge of the characteristic frequencies of the turbulence and the shear flow scales, we can estimate the time evolution of the relevant quantities. A detailed discussion of this approach to the data analysis is available [23].

In order to close the predator–prey model of turbulent-driven shear flow during the L-H transition, an analytic form for the turbulent stress verses shearing rate had to be assumed and was taken to be given by [10]

$$\langle \tilde{\nu}_r\tilde{\nu}_\theta \rangle \propto \langle \tilde{\nu}_r\tilde{\nu}_\theta \rangle \frac{V'^{\mathrm{LF}}}{1 + \alpha V'^{\mathrm{LF}^2}}.$$

These experiments permit an experimental test of this ansatz. Figure 3 below shows the time evolution of the turbulent stress plotted against the shear rate during a fast L-H transition in C-Mod inferred from the He-GPI data. These data are for a position about 1 cm inside the LCFS, which, as shown below, is the position where the peak flow drive and turbulence suppression occurs. The results show that the turbulent stress increases markedly as the shear flow begins to grow during the early portion of the L-H transition. As the shearing rate increases further, the turbulent stress reaches a peak value, and then falls as the shearing rate is increased further. The H-mode state then ensues, characterized by a strong shear and a weak turbulent stress. An examination of a number of ALCATOR C-MOD L-H transitions show a similar evolution
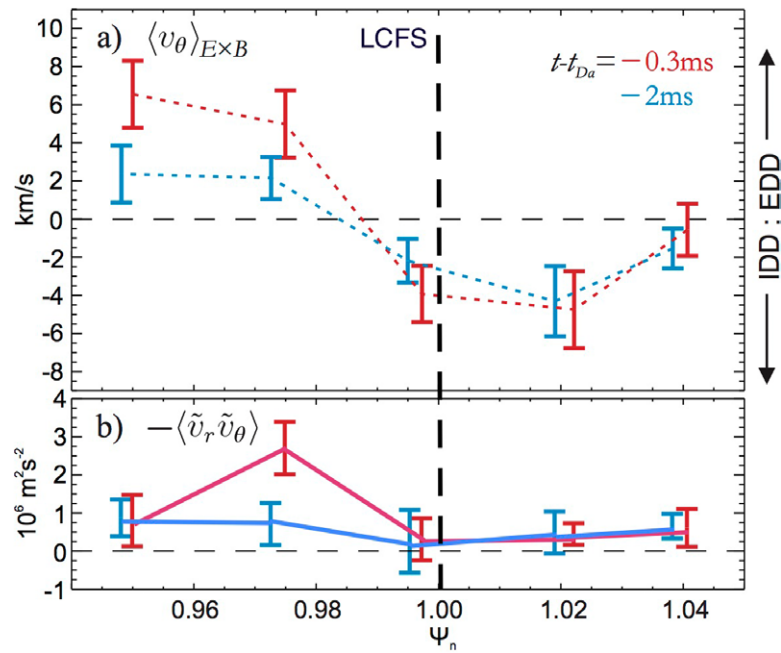
Figure 4. (a) The dashed lines show radial profile of poloidal $E \times B$ propagation speed just 2 ms before (blue) and 0.3 ms before (red) the onset of the D_α drop that is taken to indicate the moment of the L-H transition. (b) Turbulent Reynolds stress, profiles for the same two times. The radial $E \times B$ flow gradient steepens considerably in the region just inside the LCFS across the L-H transition, consistent with effects of the turbulent Reynolds stress transient observed to occur in the same region. Data from ALCATOR C-MOD. EDD/IDD denote electron/ion diamagnetic direction, respectively. The LCFS uncertainty is limited by the diagnostic resolution to approximately ± 0.01 in normalized flux units.
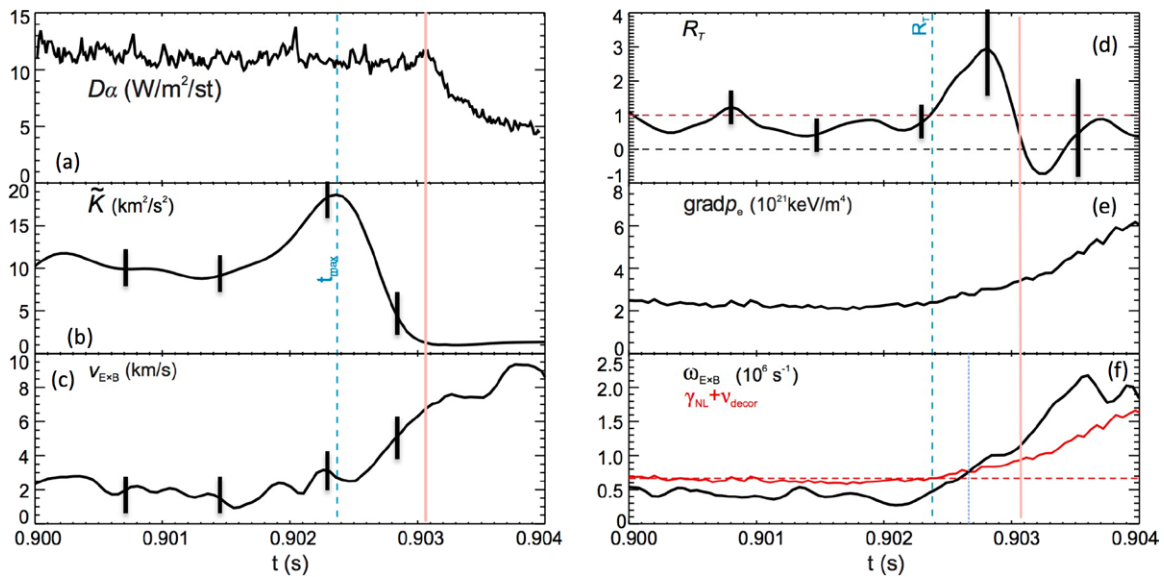
Figure 5. Evolution of (a) D_α emission, (b) edge turbulence kinetic energy, (c) sheared $E \times B$ flow, (d) normalized rate of Reynolds work, R_T, (e) grad-P_e and (f) total $E \times B$ shear rate, $\omega_{E \times B} = V'_{E \times B}$ and estimated turbulence energy input rate, given by $\gamma_{NL} + \nu_{decor}$, the onset of the D_α emission drop is shown as a vertical pink line. The onset of the turbulence energy collapse is shown as a vertical blue dashed line. Data from ALCATOR C-MOD.

of stress versus shearing rate. This behavior is consistent with the above form, providing experimental evidence that one of the key assumptions involved in the predator–prey model.

The radial gradient of this stress is the poloidally directed Reynolds force, which acts to reinforce the shear flow by steepening it. This effect can be seen in figure 4(a), which shows how the poloidal velocity profile steepens in the region just inside the LCFS at the very beginning of the L-H

transition, in the same region where a transient increase in the turbulent stress is also inferred from the GPI data (figure 4(b)). The transient in the turbulent stress occurs over a short (~1 ms) period, and thus applies a short impulse-like Reynolds force to the plasma immediately inside the LCFS.

The temporal evolution of edge turbulence, the sheared $E \times B$ flow, the normalized rate of Reynolds work R_T, grad-P_{ion}, and the shearing rate during a fast L-H transition in

an ALCATOR C-Mod are summarized in figure 5 below. As discussed above, the L-H transition is initiated by a transient increase in the turbulence amplitude and sheared $E \times B$ flow, which both occur at about 902 ms. The time of the D_α drop, which is the usual indicator of the onset of H-mode, is shown as a vertical red line at about 903 ms. About 1 ms prior to this point in time, a small burst in the edge turbulence kinetic energy is observed. At about the same time, the poloidal component of the $E \times B$ velocity is observed to begin to increase. At about 902.4 ms into the discharge, the turbulence amplitude peaks and begins to then rapidly (~300 μs) collapse. As the turbulence energy peaks and begins its collapse, the normalized rate of Reynolds work, R_T, begins to increase, exceeds unity (which is when the turbulence collapse begins), and ultimately reaches a peak value of 2–3, indicating that the rate of energy extraction of the turbulent driven $E \times B$ flow has, momentarily, exceeded the rate of energy input into the turbulence. During this whole period, the edge pressure gradient is then beginning to evolve. Note that the gradient shown here is the electron pressure gradient; however due to the high collision rates in ALCATOR C-MOD, this is essentially equivalent to the ion pressure gradient [23]. Early on in the transition sequence, the changes in the gradient are quite small. As the turbulence collapse progresses, the gradient builds, and by the time that the turbulence collapse is nearly complete, the edge pressure gradient has nearly doubled. A comparison of the $E \times B$ shear rate, $\omega_{E \times B} = V'_{E \times B}$, against the estimated turbulence energy input rate, $\gamma_{in} = \gamma_{NL} + Y_{decor}$, shows how these quantities evolve on a slower timescale as compared to the transients in the turbulence energy and Reynolds work.

The work done by the turbulence on the shear flow is consistent with the change in the shear flow energy [23]. To see this, we first used time-stationary measurements in the L-mode regime immediately preceding the transition to estimate the shear flow damping rate, $\nu_{LF} \sim 4 \times 10^3\,\mathrm{s}^{-1}$. The time evolution of the flow and its damping rate is then compared to the flow production, by comparing the terms $\partial\overline{K}/\partial t + \nu_{LF}\overline{K}$ and $P - \partial_r\overline{T}$. The results (figure 6) show reasonable agreement, indicating that the turbulent flow drive would appear to be capable of inducing the observed flow evolution.

The nonlinear flow drive is localized spatially to the region about 0.5–0.8 cm inside the LCFS, as illustrated in figure 7. The observations show that the region of turbulence suppression during the L-H transition located at and inside the LCFS (figure 7(a)). The nonlinear flow drive is localized to a narrow zone about 0.5 cm inside the LCFS (figure 7(b)). This region of flow drive is consistent with the location of the strong increase in flow shear, as shown in figure 4 above. It is interesting to note that the region where the turbulence energy is suppressed is much wider, and extends deeper into the plasma than the region of localized velocity shear and shear flow production.

A number of other recent experimental studies of the origin of the L-H transition have also been published using a similar analysis framework. Using probe arrays on EAST, Manz *et al* showed a similar picture of the transition [20]. In biased H-mode experiments on TEXTOR [27], it was also found that the H-mode onset occurred when the rate of Reynolds work was sufficiently strong to cause turbulence collapse in a biased
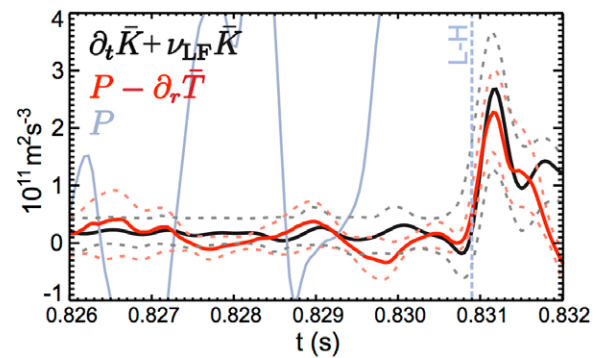

Figure 6. Time evolution of shear flow production, $P - \partial_r\overline{T}$ and flow inertia and damping, $\partial\overline{K}/\partial t + \nu_{LF}\overline{K}$ during a fast L-H transition. The fast transition occurs in this discharge at $t = 0.8309$ sec. The two terms are in reasonable agreement. The production term, P, alone does not agree with the evolution of the shear flow energy. Figure taken from [23]. Data from ALCATOR C-MOD.

H-mode experiment. In addition, that work provided elegant direct imaging of turbulent eddy tilting and stretching, illustrating the underlying mechanism that leads to the formation of a non-zero Reynolds stress that then amplifies the $E \times B$ shear flow. Analysis of the imaging data from DIII-D [33] also showed a similar picture in which turbulent eddies are elongated and distorted during the L-H transition, leading to a non-zero Reynolds stress that then induces work at a rate sufficient to lead to turbulence collapse and the formation of an edge pressure gradient. We also note that these results bear a strong resemblance to those obtained in the transition to improved Ohmic confinement obtained in the HT-6M device [34].

Comparison to turbulent simulations

Recent turbulence-based simulations of the L-H transition have also been reported [35, 36]. In both studies, turbulence-based models of the advection of pressure and vorticity are solved with certain assumptions about how, in the absence of turbulent flow drive, poloidal flows relax towards neoclassical values. In these studies the heat input was increased slowly to permit the study of the limit cycle regime that lies at the boundary between the L-mode and H-mode. In both cases, the system was found to form a region of steep edge pressure gradient and reduced or suppressed turbulence intensity. Chone' *et al* commented on the role that turbulent driven sheared flows play in starting the transition off by extracting energy from the turbulence, which then allows the pressure gradient to grow; if a sufficiently strong gradient developed before the turbulence recovered, a steep edge barrier would then develop and lock-in. In the study by Park *et al* the role of the Reynolds work in initiating the transition was explicitly examined. The results, summarized in figure 8 below, indicated that the normalized Reynolds work first exhibited a peak strong enough to extract most of the turbulent energy, and that this peaking was followed by the formation of strong mean shear flow (associated with the edge plasma pressure gradient) that satisfied the usual shear decorrelation criteria $\omega_{E \times B} > \gamma_{iin}$. Thus the
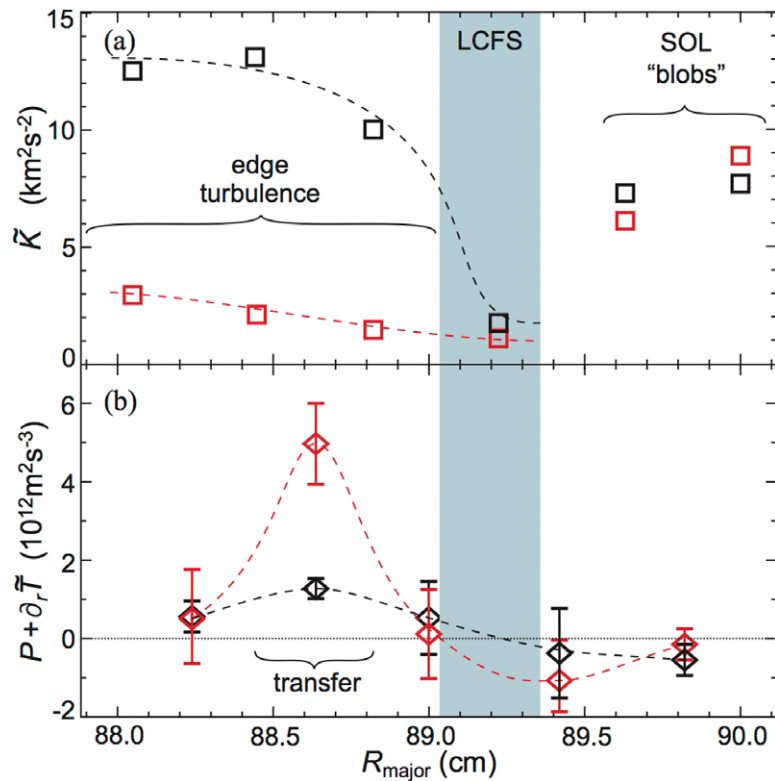
Figure 7. (a) Turbulent kinetic energy profile just before (black) and just after (red) L-H transition. (b) Nonlinear flow production profiles. Strong flow production occurs about 0.5 cm inside the LCFS, in the same region where strong turbulence energy reduction occurs. Data from ALCATOR C-MOD.
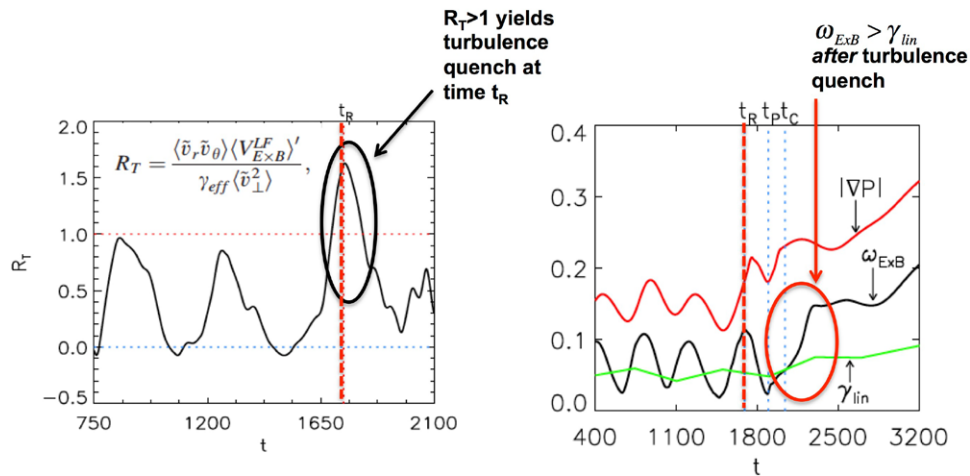

Figure 8. Left: evolution of normalized Reynolds work, R_T, during the development of an edge transport barrier. Right: evolution of the pressure gradient, mean flow shearing rate $\omega_{E \times B}$ and linear growth rate γ_{lin} in a resistive ballooning mode turbulent simulation of edge transport barrier formation. The momentary transient spike in $R_T > 1$ leads to a collapse in turbulence amplitude, allowing the edge pressure gradient to subsequently build. The shearing rate associated with the pressure gradient then subsequently satisfies the usual shear decorrelation criteria $\omega_{E \times B} > \gamma_{\mathrm{lin}}$, locking in the H-mode state. Time is normalized to major radius divided by Alfven speed, R_0/V_A. Figure adapted from [36].

turbulence collapse was determined to be associated with a transient nonlinear flow drive, and the pressure gradient then evolved in response to the change in transport so as to then allow the usual shear flow criteria to be satisfied in the new strong pedestal regime.

Making the link to macroscopic system behavior

These results show that the reduced predator–prey models capture many of the essential elements of the L-H transition, suggesting that they provide a route to link this
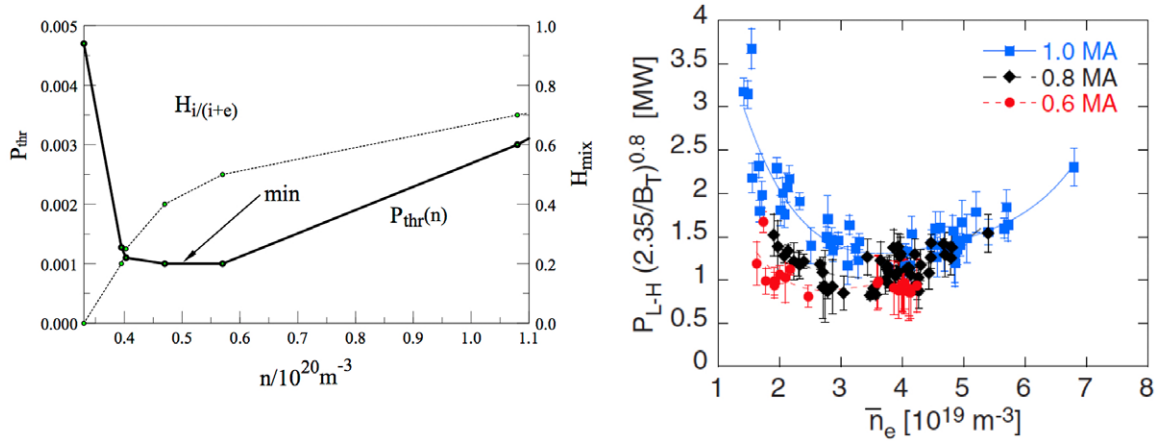
Figure 9. Left: (a) Variation of $P_{th}(n)$ with density for the given heating mix evolution $H_{i/i+e}(n)$. Figure adapted from [38]. Right: (b) variation of $P_{th}(n)$ in AUG, showing non-monotonic evolution with plasma density. Panel (b) adapted from [37].

microscopic turbulence picture of the transition with the macroscopic conditions necessary to initiate an H-mode transition. Here we briefly point out one recent extension of the predator–prey model, which can qualitatively reproduce the non-monotonic density dependence of the power threshold for the L-H transition. We then briefly summarize ideas on how other important macroscopic control parameters for the L-H transition might be understood within a similar framework.

Recent work on the AUG [37] points towards the key role played by the ion heat flux in the L-H transition. In particular, by controlling the heat input into the ion and electron channels independently, Ryter *et al* showed that the power threshold could be related to a continuous increase in the ion heat flux at the boundary of the plasma. Secondly, in a separate analysis, a correlation between the density corresponding to the transition from linear Ohmic confinement to saturated Ohmic confinement (LOC–SOC), and the density corresponding to the minimum in the L-H transition power threshold was reported [38]. The LOC–SOC transition has been linked to the development of significant collisional heat transfer between the electrons and ions. Thus this correlation also indicates that electron–ion heat transfer may also be linked to the L-H transition power threshold minimum.

Motivated by these considerations, Malkov and Diamond modified the 1D predator–prey model to now include separate electron and ion pressures, and allowed for a density dependent collisional energy exchange between the two species [38]. In addition, they parameterized the relative fraction of heating to the two species and explored how this could then affect the power threshold evolution with plasma density. The relative roles of turbulent driven shear flow and ion diamagnetic mean shear flows were left unchanged from previous work. The results showed that, provided the relative fraction of heating to the ions, $H_{i/i+i}(n)$ was an increasing function on density, then a pronounced minimum in the power threshold verses density, $P_{th}(n)$ could be obtained, as shown in figure 9(a), in qualitative agreement with the experimental results in figure 9(b).

Discussion

At first glance, these results seem promising and suggest that an understanding of the origins of the L-H transition might be nearly in hand. However, there are a number of observations and questions that remain that must be faced and addressed before any such conclusion can be reached. For example, work in the MAST did not show evidence for an evolution of E_r or its shear prior to the L-H transition in that device [39]. Similarly, recent work in the ASDEX UG shows no evidence for a transient departure of the $E \times B$ shearing from the expected neoclassical value or, in the parlance of the terminology used in this paper, from the ion diamagnetic drift [40]. These ASDEX UG results also show that the background gradient evolution may also evolve on the sort of fast timescales associated with the turbulence evolution. Indeed, an examination of figure 5 shows that the pressure gradient build-up begins nearly as soon as the turbulence amplitude collapses. Perhaps the scale separation assumed in the models discussed here would break down, and gradient evolution could contribute to turbulent stress evolution. Whether or not this can resolve these apparent discrepancies across different experiments is unknown at present and must be confronted. It might be useful to use the turbulent data analysis approaches described here to study the possible role of turbulent-driven shear flows in these other devices. Conversely, it would be useful to obtain high spatio-temporal resolution data in, e.g. ALCATOR C-Mod, DIII-D, and other devices to determine if there is a fast, transient departure of E_r determined from the ion pressure gradient alone.

Second, the role of GAMs in the L-H transition is not fully understood. The effects of compressibility in toroidal geometry have been shown theoretically to strongly damp zonal flows by coupling them to GAMs, which are, in turn, strongly damped [41, 42]. As a result, toroidal effects are expected to increase the effective inertia of the plasma poloidal rotation in a torus, thereby reducing the effectiveness of the Reynolds stress in driving poloidal rotation and the associated sheared $E \times B$ flow [43]. In the face of these theoretical

expectations, experiments either show that as the L-H transition is approached, the GAM signature dies away while the low-frequency sheared zonal flow becomes quite pronounced [28], or shows no evidence for the role of GAMs during the approach to the L-H transition [23, 44]. Furthermore, quantitative estimates of the Reynolds flow drive including these GAM effects, or using an empirically derived flow damping rate have been shown to be consistent with the observed plasma flows [23, 44].

Making the situation even more complex, recent observations of ALCATOR C-Mod L-mode to I-mode transitions clearly show that the GAM is nonlinearly generated at the moment of the L–I transition, and in fact no low frequency zonal flow occurs in this case [30]. There is no experimental understanding of how the plasma chooses between a ZF-mediated L-H transition, and a GAM-mediated L–I transition. These necessarily brief considerations clearly show that additional work is needed to resolve the role of GAMs and GAM flow damping effects in the L-H transition; this might also lead to an improved understanding of access to other improved confinement regimes (e.g. I-mode) that are potentially more attractive than the H-mode.

There are also other macroscopic scaling behaviors that need to be explained if this physics picture is correct. Perhaps the most obvious is the origin of the favorable ion grad-$B \times B$ drift direction of the L-H transition, in which the power threshold is observed to be lower when the ion grad-$B \times B$ drift direction is pointed towards the X-point. It has been proposed [45] that magnetic shear provides a second means to locally tilt and stretch turbulent eddies, resulting in the formation of a turbulent stress. In the presence of an up–down asymmetry in the fluctuation amplitude induced, e.g. by the presence of an X-point, then the resulting flux-surface averaged poloidal momentum balance then contains two components to the surface averaged stress; one associated with the magnetic shear, and one associated with the $E \times B$ shear. It was then shown that in the case of favorable drift, these two terms added, while in the case of unfavorable shear they competed with each other. Subsequent work provided some initial evidence in support of this picture [46] but additional work is needed to determine if this picture is indeed correct.

We also note that experiments show that the power threshold depends sensitively upon other experimental parameters, e.g. divertor X-point height [47], main plasma isotope, and wall conditioning [37]. Further work is needed to determine if and how these observations could be explained within the context of the physics model discussed here. Finally, the extended power threshold model of Malkov and Diamond [38] is based on collisional heat exchange between the electron and ion species. This naturally raises the question: How does the system then behave in nearly collisionless plasmas that will be found in the ITER? Will anomalous energy exchange occur, in which turbulent fluctuations play the role of collisions to affect a significant exchange of energy in these conditions? Further work is clearly needed to address these important questions.

Conclusions

Results from recent experiment and numerical simulation point towards a picture of the L-H transition, in which edge shear flows interacting with edge turbulence create the conditions needed to produce a non-zero turbulent Reynolds stress at and just inside the LCFS during L-mode discharges. This stress acts to reinforce the shear flow at this location and the flow drive gets stronger as heating is increased. The L-H transition ensues when the rate of work done by this stress is strong enough to drive the shear flow to large values, which then grows at the expense of the turbulence intensity. The drop in turbulent intensity momentarily reduces the heat flux across the magnetic flux surface, which then allows the edge plasma pressure gradient to build. A sufficiently strong ion pressure gradient then locks in the H-mode state. These results are in general agreement with previous reduced 0D and 1D predator prey models. A number of open questions and unexplained observations are identified, and must be addressed and resolved in order to build a physics-based model that can yield predictions of the macroscopic conditions needed for accessing H-mode.

References

[1] Wagner F *et al* 1982 Regime of improved confinement and high-beta in neutral-beam-heated divertor discharges of the Asdex tokamak *Phys. Rev. Lett.* **49** 1408–12

[2] Burrell K H 1997 Effects of $E \times B$ velocity shear and magnetic shear on turbulence and transport in magnetic confinement devices *Phys. Plasmas* **4** 1499–518

[3] Wagner F 2007 A quarter-century of H-mode studies *Plasma Phys. Control. Fusion* **49** B1–33

[4] Martin Y R, Takizuka T and I. C. H. M. T. Databas 2008 *11th IAEA Technical Meeting on H-Mode Physics and Transport Barriers* vol 123, ed T Takizuka

[5] Carlstrom T N, Gohil P, Watkins J G, Burrell K H, Coda S, Doyle E J, Groebner R J, Kim J, Moyer R A and Rettig C L 1994 Experimental survey of the L-H transition conditions in the Diii-D tokamak *Plasma Phys. Control. Fusion* **36** A147–52

[6] Carlstrom T N and Groebner R J 1996 Study of the conditions for spontaneous H(high)-mode transitions in DIII-D *Phys. Plasmas* **3** 1867–74

[7] Zohm H 1994 Dynamic behavior of the L-H transition *Phys. Rev. Lett.* **72** 222–5

[8] Diamond P H, Liang Y M, Carreras B A and Terry P W 1994 Self-regulating shear-flow turbulence—a paradigm for the L to H transition *Phys. Rev. Lett.* **72** 2565–8

[9] Colchin R J *et al* 2002 Slow L-H transitions in DIII-D plasmas *Phys. Rev. Lett.* **88** 255002

[10] Kim E J and Diamond P H 2003 Zonal flows and transient dynamics of the L-H transition *Phys. Rev. Lett.* **90** 185006

[11] Estrada T *et al* 2009 Sheared flows and transition to improved confinement regime in the TJ-II stellarator *Plasma Phys. Control. Fusion* **51** 124015

[12] Estrada T, Happel T, Hidalgo C, Ascasibar E and Blanco E 2010 Experimental observation of coupling between turbulence and sheared flows during L-H transitions in a toroidal plasma *Europhys. Lett.* **92** 35001

[13] Estrada T, Ascasibar E, Blanco E, Cappa A, Castejon F, Hidalgo C, van Milligen B P and Sanchez E 2015 Limit cycle oscillations at the L-I-H transition in TJ-II plasmas: triggering, temporal ordering and radial propagation *Nucl. Fusion* **55** 063005

[14] Conway G D, Angioni C, Ryter F, Sauter P, Vicente J and A. U. Team 2011 Mean and oscillating Plasma flows and turbulence interactions across the L-H confinement transition *Phys. Rev. Lett.* **106** 065001

[15] Schmitz L 2012 Role of zonal flow predator-prey oscillations in triggering the transition to H-mode confinement *Phys. Rev. Lett.* **108** 155002

[16] Xu G S *et al* 2014 Study of the L-I-H transition with a new dual gas puff imaging system in the EAST superconducting tokamak *Nucl. Fusion* **54** 013007

[17] Miki K, Diamond P H, Guercan O D, Tynan G R, Estrada T, Schmitz L and Xu G S 2012 Spatio-temporal evolution of the L-I-H transition *Phys. Plasmas* **19** 092306

[18] Miki K, Diamond P H, Hahn S H, Xiao W W, Guercan O D and Tynan G R 2013 Dynamics of stimulated L-H transitions *Phys. Plasmas* **20** 082304

[19] Miki K, Diamond P H, Hahn S H, Xiao W W, Gurcan O D and Tynan G R 2013 Physics of Stimulated L-H Transitions *Phys. Rev. Lett.* **110** 195002

[20] Manz P *et al* 2012 Zonal flow triggers the L-H transition in the experimental advanced superconducting tokamak *Phys. Plasmas* **19** 4737612

[21] Manz P, Xu M, Fedorczak N, Thakur S C and Tynan G R 2012 Spatial redistribution of turbulent and mean kinetic energy *Phys. Plasmas* **19** 012309

[22] Tynan G R *et al* 2013 Turbulent-driven low-frequency sheared $E \times B$ flows as the trigger for the H-mode transition *Nucl. Fusion* **53** 073053

[23] Cziegler I, Tynan G R, Diamond P H, Hubbard A E, Hughes J W, Irby J and Terry J L 2014 Zonal flow production in the L-H transition in Alcator C-Mod *Plasma Phys. Control. Fusion* **56** 075013

[24] Ritz C P, Bengtson R D, Levinson S J and Powers E J 1984 Turbulent structure in the edge plasma of the text tokamak *Phys. Fluids* **27** 2956-9

[25] Hidalgo C *et al* 1991 Plasma fluctuations near the shear-layer in the atf torsatron *Nucl. Fusion* **31** 1471-8

[26] Carter T A and Maggs J E 2009 Modifications of turbulence and turbulent transport associated with a bias-induced confinement transition in the large plasma device *Phys. Plasmas* **16** 012304

[27] Shesterikov I, Xu Y, Tynan G R, Diamond P H, Jachmich S, Dumortier P, Vergote M, Van Schoor M, Van Oost G and T. Team 2013 Experimental evidence for the Intimate interaction among sheared flows, Eddy structures, Reynolds stress, and zonal flows across a transition to improved confinement *Phys. Rev. Lett.* **111** 055006

[28] Xu M *et al* 2012 Frequency-resolved nonlinear turbulent energy transfer into zonal flows in strongly heated L-mode plasmas in the HL-2A tokamak *Phys. Rev. Lett.* **108** 245001

[29] Nold B, Ribeiro T T, Ramisch M, Huang Z, Mueller H W, Scott B D, Stroth U and A. U. Team 2012 Influence of temperature fluctuations on plasma turbulence investigations with Langmuir probes *New J. Phys.* **14** 063022

[30] Cziegler I *et al* 2013 Fluctuating zonal flows in the I-mode regime in Alcator C-Mod *Phys Plasmas* **20** 055904

[31] Cziegler I, Terry J L, Hughes J W and LaBombard B 2010 Experimental studies of edge turbulence and confinement in Alcator C-Mod *Phys Plasmas* **17** 056120

[32] Xu M, Tynan G R, Holland C, Yan Z, Muller S H and Yu J H 2009 Study of nonlinear spectral energy transfer in frequency domain *Phys Plasmas* **16** 042312

[33] Yan Z, McKee G R, Fonck R, Gohil P, Groebner R J and Osborne T H 2014 Observation of the L-H confinement bifurcation triggered by a turbulence-driven shear flow in a tokamak plasma *Phys. Rev. Lett.* **112** 125002

[34] Xu Y H, Yu C X, Luo J R, Mao J S, Liu B H, Li J G, Wan B N and Wan Y X 2000 Role of Reynolds stress-induced poloidal flow in triggering the transition to improved ohmic confinement on the HT-6M tokamak *Phys. Rev. Lett.* **84** 3867-70

[35] Chone L, Beyer P, Sarazin Y, Fuhr G, Bourdelle C and Benkadda S 2014 L-H transition dynamics in fluid turbulence simulations with neoclassical force balance *Phys. Plasmas* **21** 070702

[36] Park G Y, Kim S S, Jhang H, Diamond P H, Rhee T and Xu X Q 2015 Flux-driven simulations of turbulence collapse *Phys Plasmas* **22** 032505

[37] Ryter F *et al* 2013 Survey of the H-mode power threshold and transition physics studies in ASDEX upgrade *Nucl. Fusion* **53** 113003

[38] Malkov M A, Diamond P H, Miki K, Rice J E and Tynan G R 2015 Linking the micro and macro: L-H transition dynamics and threshold physics *Phys. Plasmas* **22** 032506

[39] Meyer H *et al* 2011 L-H transition and pedestal studies on MAST *Nucl. Fusion* **51** 113011

[40] Cavedon T P M, Viezzer E, Birkenmeirer G, Happel T, Laggner F, Prosiazhniuk D, Ryter F, Stroth U and the ASDEX Upgrade Team 2015 *Presented at the 2015 European Physical Society Meeting (Lisbon Portugal, 22–26 June 2015)* (unpublished)

[41] Scott B D 2005 Energetics of the interaction between electromagnetic $E \times B$ turbulence and zonal flows *New J. Phys.* **7** 92

[42] Hallatschek K 2007 Nonlinear three-dimensional flows in magnetized plasmas *Plasma Phys. Control. Fusion* **49** B137-48

[43] Kobayashi T *et al* 2013 Spatiotemporal structures of edge limit-cycle oscillation before L-to-H transition in the JFT-2M tokamak *Phys. Rev. Lett.* **111** 035002

[44] Xu G S *et al* 2014 Dynamics of L-H transition and I-phase in EAST *Nucl Fusion* **54** 103002

[45] Fedorczak N, Diamond P H, Tynan G and Manz P 2012 Shear-induced Reynolds stress at the edge of L-mode tokamak plasmas *Nucl Fusion* **52** 103013

[46] Fedorczak N, Ghendrih P, Hennequin P, Tynan G R, Diamond P H and Manz P 2013 Dynamics of tilted eddies in a transversal flow at the edge of tokamak plasmas and the consequences for L-H transition *Plasma Phys. Control. Fusion* **55** 124024

[47] Hughes J 2015 *Presented at the US-E.U. Transport Task Force Meeting (Salem, MA, 2015)* (unpublished)